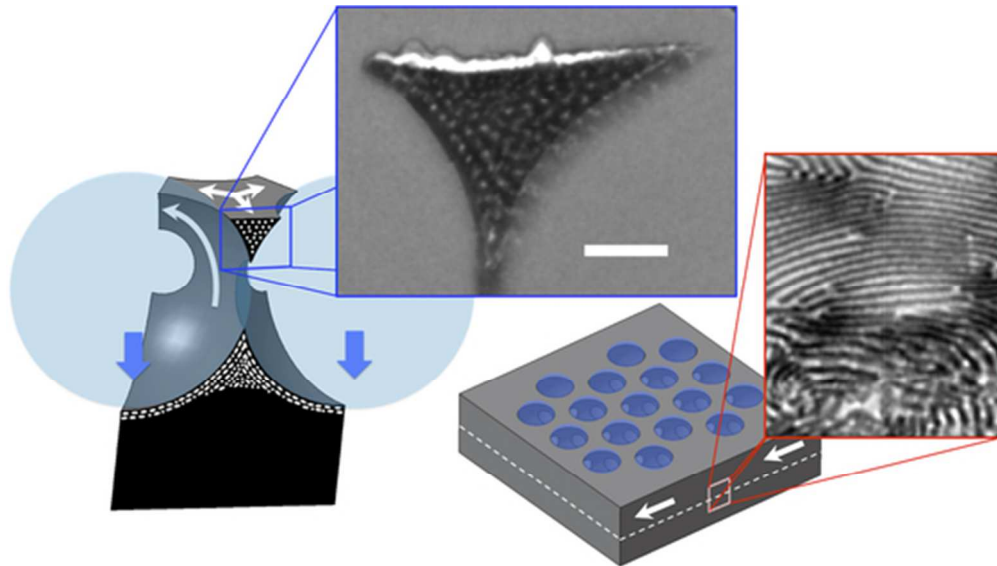




When block copolymer self-assembly in hierarchically ordered honeycomb films depicts the breath figure process

Journal:	<i>Soft Matter</i>
Manuscript ID	SM-ART-07-2015-001774.R1
Article Type:	Paper
Date Submitted by the Author:	16-Oct-2015
Complete List of Authors:	Escalé, Pierre; Université de Pau et des Pays de l'Adour, IPREM-EPCP Save, Maud; University of Pau, Chemistry Billon, Laurent; IPREM EPCP UMR 5254, Chemistry Ruokolainen, Janne; Aalto University School of Science, Rubatat, Laurent; Université de Pau et des Pays de l'Adour, IPREM-EPCP



The detailed observation of the block copolymer self-assembly within a micrometer length scale honeycomb films obtained by the Breath Figure process, points out the structural interplays between both length-scales and establishes the potential interest of using the kinetically trapped block copolymer self-organization as an imprint to elucidate the complex film formation.

47x26mm (300 x 300 DPI)



When block copolymer self-assembly in hierarchically ordered honeycomb films depicts the breath figure process

Pierre Escalé,^{a,†} Maud Save,^a Laurent Billon,^{*a} Janne Ruokolainen^b and Laurent Rubatat^{**a}

Received 00th January 20xx,
Accepted 00th January 20xx

DOI: 10.1039/x0xx00000x

www.rsc.org/

Nowadays, a challenge for the preparation of hierarchically ordered materials is the control of concomitant and interacting self-organization processes occurring in time at different length scales. In the present paper, Breath Figure process is combined with block copolymers nano-phase segregation to elaborate hierarchically structured honeycomb porous films. The copolymer ordering, at the nanometer length scale, is observed and described in details with respect to the array of pores of micrometer dimension, hence pointing out the structural interplays between both length-scales. The study is focused on two diblock copolymers made of polystyrene and poly(*tert*-butyl acrylate) (PS-*b*-PtBA) with compositions producing lamellae or hexagonal packing of cylinders at thermodynamical equilibrium. Transmission Electron Microscopy completed with Small and Ultra Small Angle Scattering are performed to evidence the inner morphologies of the honeycomb. The structural data are discussed in the light of the honeycomb film formation process establishing the interest of using the kinetically trapped block copolymer self-organization as an imprint to elucidate the complex Breath Figure process.

Introduction

Since the last 15 years it has been demonstrated that the so-called Breath Figure process is a simple, inexpensive and robust method for preparing polymeric honeycomb (HC) films exhibiting an array of pores of micrometer size.^{1–7} Breath Figure occurs when water vapour condenses onto a cold surface. In the present case the surface is an evaporating polymer solution, which has the advantage of fixing the figures (*i.e.* water droplets) in the polymer film.^{1, 2} Recently, a group from Fujifilm have demonstrated the possibility to produce high quality HC films with dimension of 20 cm x 20 cm, allowing their technological transfer with high applicative potentials.^{8, 9} By now, most of the physical mechanisms occurring during the film formation are identified.⁷ However the complete description of the relatively fast process toward the kinetically trapped micrometer structure is not fully achieved; mainly due to the experimental complexity to observe the water droplet dynamics during the solvent evaporation. Though, based on *in situ* and time resolved confocal microscopy observations, Srinivasarao *et al.*^{10, 11} have proposed a three steps process: (i) the water droplet nucleation and growth on the cold evaporating polymer solution; (ii) the self-organization of the water droplets into ordered hexagonal lattices; and finally (iii) the sinking of the water droplet arrays in the solution before the total solvent evaporation. Additional description of the collective droplet

motions during the film formation has been recently proposed by Yamazaki *et al.*⁹ with the concept of tectonic; in which the HC film defects are the result of a convergence and divergence lateral motion of droplets arrays.

The simplicity of the Breath Figure method has led to the preparation of films using a wide range of polymers and different macromolecular architectures including block copolymers leading potentially to hierarchical morphologies.^{3, 5, 6} From the applications point of view there is a strong interest in hierarchical structures, especially within biomimetic approaches, to design surfaces with advanced adhesion,¹² or the self-cleaning properties.^{13, 14} To achieve the multi length scale structure via the Breath Figure process, the block copolymers have to be soluble in appropriate organic solvents,⁶ and the blocks have to be immiscible. Also, other parameters such as polarity and glass transition temperature of the blocks can affect the quality of the HC structure.¹⁵ Nevertheless, very few studies have demonstrated the nanostructures brought by the block copolymers within the HC walls. Indeed, the challenge for the preparation of hierarchically ordered films is the control of concomitant and interacting self-organization processes occurring in time at different length scales. Hayakawa and Horiuchi have reported the ordering of semi rod-coil copolymers into cylindrical domains restricted at the close vicinity of the pores.¹⁶ Those materials are expected to find applications in electronic devices, photonic band-gap and sensors. Later, using regular coil triblock copolymers, Munoz-Bonilla *et al.* reported a nano-phase separation at the bottom of erratically ordered pores on

^a Université de Pau et des Pays de l'Adour, Hélioparc, IPREM Equipe de Physique et Chimie des Polymères, UMR 5254 CNRS, 2 Avenue du Président Angot, 64053 Pau, France. E-mails: laurent.rubatat@univ-pau.fr, laurent.billon@univ-pau.fr

^b Department of Applied Physics, Aalto University, P.O. Box 11100, FI-00076 Aalto, Finland.

[†] Present Adresse: CANOE, Cheminnoy, 16, avenue Pey Berland, 33600, Pessac, France.

spin casted films, expected to present switching tribological properties.¹⁷ More recently, our group has evidenced the hierarchical structure on the surface and in the walls of the HC films prepared from poly(alkyl acrylate)-*b*-polystyrene block copolymers¹⁵ or amphiphilic diblock copolymers¹⁸⁻²⁰ which demonstrated respectively adhesion and switching wettability properties.

The present paper proposes a detailed investigation of the hierarchical morphology within the polymer films prepared by the Breath Figure process involving a diblock copolymer. The interplays between both length scale structures are pointed out to give insight into the Breath Figure process. The copolymers, composed of polystyrene and poly(*tert*-butyl acrylate) blocks (PS-*b*-PtBA), are selected to induce different thermodynamical equilibrium morphologies, *i.e.* lamellar and hexagonal packing of cylinders. Transmission Electron Microscopy (TEM) is intensively used on films sections to observe the inner morphologies, completed with Small and Ultra Small Angle Scattering (SANS, SAXS & USAXS) data. To the best of our knowledge, this is the first time that kinetically trapped nanostructures of block copolymers are observed in the entire HC film (*i.e.* around the pores but also deep under the pores) and used as an imprint to elucidate the complex Breath Figure film formation process.

Experimental section

Materials

Well-defined high molecular weight poly(*tert*-butyl acrylate) - *block* - polystyrene (PtBA-*b*-PS) diblock copolymers were synthesized by Nitroxide Mediated controlled free-radical Polymerization, NMP. The characteristics of the resulting block copolymers are presented in Table 1.

Preparation of the HC films

The preparation of the HC films through the Breath Figure process was performed in a Perspex glove box at room temperature (20°C) with relative humidity ranging from 35 to 45%. The humid airflow on the evaporating solution was set at 2 L.min⁻¹. The copolymers were first dissolved in carbon disulfide (CS₂, Aldrich, 99.9%) to obtain a concentration of 5 g.L⁻¹ and 100 mL of the solution were directly cast on a glass substrate. The HC films are usually obtained within less than 1 minute.

Preparation of the continuous films

The diblock copolymer solutions, 5 g L⁻¹ of polymer in toluene (Aldrich, anhydrous 99.8%) were cast into Teflon recipients. After the complete evaporation of solvent, the bulk films were thermally annealed for 48 h under vacuum at 120°C, *i.e.* above block glass transition temperatures, *T_g* (45°C and 100°C for PtBA and PS, respectively).

Table 1. Characteristics of the PtBA-*b*-PS diblock copolymers used for the film formation. The χ value is estimated from the solubility parameters assuming a symmetric composition.¹⁵

Name	Weight fraction (tBA : S)	Mn (g.mol ⁻¹)	Mw/Mn	N	χ N (25°C)
P _{LAM.}	65 : 35	81 470	1.4	690	90
P _{CYL.}	40 : 60	68 800	1.35	630	81

Optical Microscopy

Pictures were taken in reflection mode with a Leica DM/LM microscope equipped with Leica DFC280 video camera. The regular image treatments were performed with the Image Manager IM50 software. The Voronoï treatment and the analysis were performed with Igor Pro software (WaveMetrics, Inc.) using a homemade code. The analysis is based on the pictures from Fig. 1.

Small Angle Scattering

The spectra are plotted as a function of the scattering vector q defined as $q = 4\pi/\lambda \sin(\theta/2)$ with θ the scattering angle. Standard data corrections were applied depending on the neutron or X-ray scattering methods; the scattering intensities are given in arbitrary units. The Small Angle X-ray Scattering (SAXS) and Ultra Small Angles X-rays Scattering (USAXS) were collected at the European Synchrotron Radiation Facility (ESRF, Grenoble, France) on the ID02 beamline. The SAXS data were collected by a two-dimensional detector positioned at three different sample-to-detector distances, 0.8, 2.5 and 10 m, using a 0.99 Å wavelength beam. The USAXS data were collected at ID02 on a Bonse & Hart camera with a wavelength of 0.99 Å as well. The SANS measurements (from reference¹⁵) were performed at Laboratoire Leon Brillouin (LLB, CEA-Saclay, France) on the PAXY beamline. For the SANS experiment the HC film samples were prepared by stacking identical HC films on top of each other, up to 20 films in order to have a sufficient irradiated volume.

Transmission Electron Microscopy

Transmission electron microscopy (TEM) was carried out using a Jeol JEM-3200FSC field emission microscope operating at 300 kV voltage. The images were taken in bright field mode and using zero loss energy filtering (omega type) with the slit with of 20 eV. Micrographs were recorded using Gatan Ultrascan 4000 CCD camera. The specimen temperature was maintained at -187°C during the imaging. Samples were embedded in epoxy at room temperature (Struers Specifix) and thin sections (~70 nm) were cut at room temperature by Leica EM UC7 microtome using a 25° Diatome diamond knife. The sections were collected on 300 mesh lacey carbon grids.

Results

Micrometer Length Scale Morphology Observed by Optical Microscopy

The HC structure was observed by mean of optical microscopy, two representative pictures collected on both samples are presented on Fig. 1. Sample P_{LAM} , presents a poor long range ordering of the pores contrary to P_{CYL} , which exhibits a hexagonal packing with grains size of few tens micrometers. A Voronoï analysis is performed to provide the pore-to-pore distance distribution and the distribution of the number of first neighbours for each pores.^{11, 21} The results are displayed on Fig. 2.

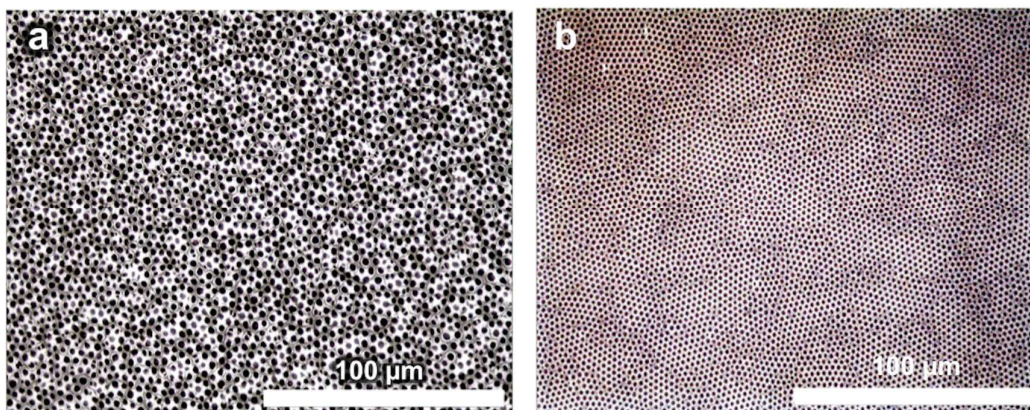


Fig. 1 Optical microscopy images acquired on HC films made from polymer P_{LAM} . (a) and P_{CYL} . (b).

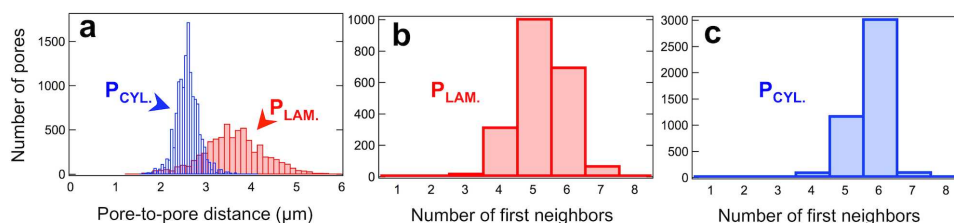


Fig. 2 Distributions of the pore-to-pore distances for samples P_{LAM} and P_{CYL} (a). Distributions of the pores' first neighbor number for sample P_{LAM} . (b) and P_{CYL} (c).

The pore-to-pore average distances are 3.6 μm for P_{LAM} and 2.6 μm for P_{CYL} with standard deviation of 0.72 and 0.26 μm respectively. The number distribution of first neighbours for each pore is sharp and centre on 6 for P_{CYL} , contrary to P_{LAM} , which confirms the direct image observation. To quantify the quality of the HC ordering the entropy, S , is calculated through the following expression:¹¹ $S = -\sum P_z \ln(P_z)$, with P_z the probability of a pore to have z neighbours; the smaller the value of S is, the higher the degree of order is. As expected, a lower entropy value is obtained for sample P_{CYL} , 0.818 exhibiting a higher ordering than P_{LAM} , 1.185.

Nanometer Length Scale Morphology Investigated by Small Angle Scattering

SAXS was performed on the continuous and HC films made from both copolymers. The SAXS curve measured on the temperature annealed continuous film P_{LAM} reveals a lamellar morphology, with a first order peak at $q^* = 8.5 \times 10^{-2} \text{ nm}^{-1}$ followed by peaks at 2, 3 and $4q^*$, indicated by the arrows on Fig. 3. The q^* measurement indicates a lamellar-to-lamellar distance of 73.4 nm ($d = 2\pi/q^*$). On the other hand, the SAXS curve collected on the temperature annealed P_{CYL} continuous film, indicates a hexagonal packing of cylinders; with a first order peak at $q^* = 1.6 \times 10^{-1} \text{ nm}^{-1}$ and peaks at $\sqrt{3}$ and $\sqrt{7}q^*$ as pointed by the arrows on Fig. 3. The expected $2q^*$ peak is most probably attenuated by a form factor minimum. The q^* peak position indicates a cylinder-to-cylinder distance of 45.3 nm ($d = 4\pi/\sqrt{3}q^*$). The cylinders are PtBA rich domains within a PS rich matrix, according to the copolymer composition, *i.e.* 40 %wt of *tert*-butyl acrylate and 60 %wt of styrene. The SAXS spectra measured on the HC films are displayed on Fig. 3. Both curves present well-marked q^{-4} slopes indicating sharp interfaces (*i.e.* Porod regime), nevertheless there isn't structural peak. The most probable explanation is the weak PS/PtBA SAXS contrast compared to the predominant scattering arising from the polymer/void interface. Extended SAXS at larger angles and USAXS were performed on the HC film made of polymer P_{CYL} . The q^{-4} power law is pursuing at larger and smaller angles until it fall off at about $q = 1 \times 10^{-2} \text{ nm}^{-1}$. This extended scattering curve is well fitted with the Debye-Anderson-Brumberger model corresponding to 2 phases system.²² The fitting curve is presented on Fig. 3 (dashed black line) using a characteristic length of 130 nm. This dimension is attributed to the averaged dimension of the polymeric walls between the pores. On the same curve, a weak peak is observed at $q = 4 \times 10^{-3} \text{ nm}^{-1}$ and attributed to the pore-to-pore distance. A dimension of 1.8 μm is estimated, considering a hexagonal packing of pores, this value is in the order of magnitude of the optical microscopy measurement. SANS spectra collected on both HC films exhibit the expected structural peaks, as the signatures of the block copolymer self-organization (Fig. 3).

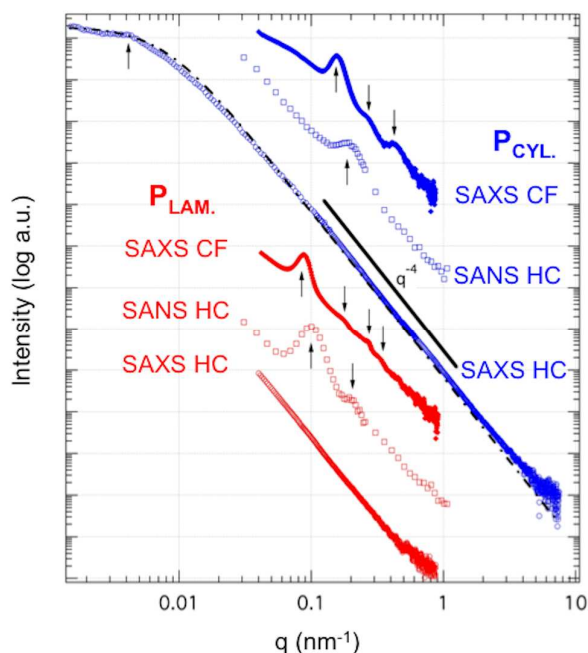


Fig. 3 Log-log plot of SAXS, USAXS and SANS scattered intensity (in arbitrary unit) as function of the scattering vector, q (in nm^{-1}). The spectra are translated vertically for sake of clarity. The red and blue curves correspond respectively to sample P_{LAM} and P_{CYL} . Solid diamonds represent the temperature annealed continuous films (CF) measured by SAXS. Open squares represent HC films measured by SANS. Open circles represent HC films measured by SAXS and completed by USAXS for sample P_{CYL} . The upward arrows are pointing the first order peaks and the downward ones the higher order ones. The dashed black line represents the fitting curve of the SAXS and USAXS data collected on P_{CYL} HC film using the Debye-Anderson-Brumberger model.

The SANS spectra measured on P_{LAM} HC film reveals a first order peak at $q^* = 1 \times 10^{-1} \text{ nm}^{-1}$ and the second order at $2q^*$. This is the signature of nano-phase segregation of the copolymer into a lamellar morphology with a relatively elevated degree of ordering. From the q^* position, the lamella-to-lamella distance is evaluated at 62.8 nm. The TEM pictures will confirm the lamellar morphology and the dimension (Fig. 4). On the other hand, the P_{CYL} HC film SANS spectra reveals a single peak located at $1.93 \times 10^{-1} \text{ nm}^{-1}$. That corresponds to a Bragg distance of 32.5 nm and indicates a phase-segregated morphology without specific long range ordering, also confirmed by the TEM pictures (Fig. 5).

Multi-Length Scale Approach by Transmission Electron Microscopy

TEM is used on cryo-ultramicrotomed sections of HC films for a direct visualization of the inner structure in between the pores and also deep under the pores. The pictures collected on different regions of P_{LAM} HC film (Fig. 4) confirm the SANS data with a highly ordered lamellar morphology. It is worth to note that this ordering is not uniform over the entire HC section. There is repeatedly a layer at the bottom of the film exhibiting a short range ordering of the lamellae as shown in region 2 on Fig. 4 b & d. The thickness of this layer ranges between 1 to 2

μm . On contrary, in region 1, at the vicinity of the pore, a long range ordering is noticed. In addition, only sections of lamellae are observed, indicating a preferential orientation of the lamellae following the pore curvature (*i.e.* the former water/polymer solution interface). This orientation propagates into the film bulk over about $1\ \mu\text{m}$. In the thin polymer walls between two pores (Fig. 4 c) and also at the top of the walls, the lamellae orientations tend to be preserved at the vicinity of the interface (polymer/void) and are frustrated by confinement effects in the bulk as shown on Fig. 4 c, d & e. To attempt the chemical nature determination of the polymer located at the interface, RuO_4 contrast agent is employed to selectively stain the polystyrene phase (Fig. 4 d & e); the PS domains appear darker and the PtBA domains brighter than the resin on the TEM pictures.[†] Fig. 4 e shows that the polystyrene lamellae are preferentially located at the interface.

The TEM images collected on the sample RuO_4 stained P_{CYL} are displayed on Fig. 5. The pictures reveal a phase separation between worm-like PtBA rich domains (brighter grey) and the PS rich matrix (darker grey) with a poor long range ordering. This is in agreement with the neutron scattering analysis. Analogously to P_{LAM} , the polystyrene matrix is preferentially located at the interface void/polymer (Fig. 5 b). A careful

observation of the TEM images (Fig. 5) evidenced the orientational inhomogeneity of the worm-like domains, which is correlated with the location in the HC film section. To facilitate the description of the various orientations, four regions of interest are identified. (i) Looking cautiously at the pore bases, close to the void/polymer interface, on Fig. 5 a & b (right inset blowups), aligned objects following the curvature of the interface are present. (ii) The entire continuous film underneath the porosity does not exhibit an obvious structural heterogeneity contrary to sample P_{LAM} . Though, two-dimensional Fast Fourier Transforms (2D FFT) are performed in three different regions of the P_{CYL} HC film and reveal a continuous variation of the structure anisotropy (Fig. 6). An important anisotropy is observed in the vicinity of the void/polymer interface, where the aligned objects fitting the curvature are observed. Deeper in the film this anisotropy tends to vanish gradually from region 1 to 3 (Fig. 6). (iii) The top parts of the HC film exhibit a regular orientation perpendicularly to the pore interface as pointed by the blue arrows on Fig. 5 d and e. (iv) On the other hand, the isolated top parts represented on Fig. 5 c exhibit a persistent orientation of the worm-like domains orthogonally to the sample section, since only isotropic domain sections are visible.

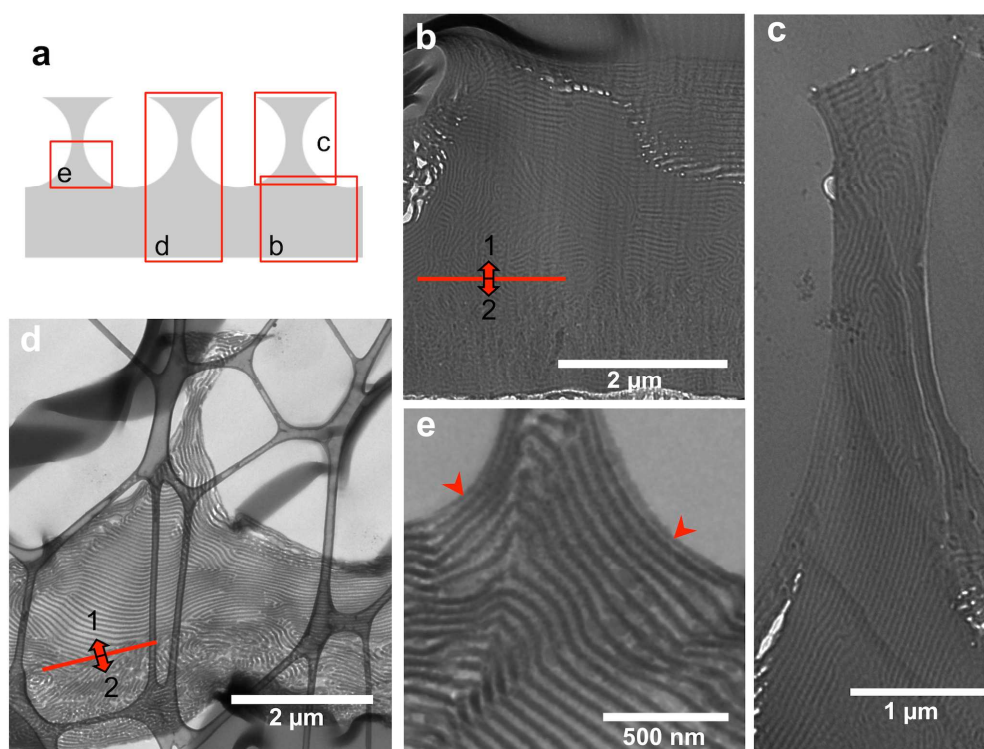


Fig. 4 Schematic representation of a HC film section (a) and cryo-TEM images collected on P_{LAM} HC film without staining (b & c) and RuO_4 stained (d & e). Regions 1 & 2 in pictures b & d correspond respectively to the long and short range ordered regions.

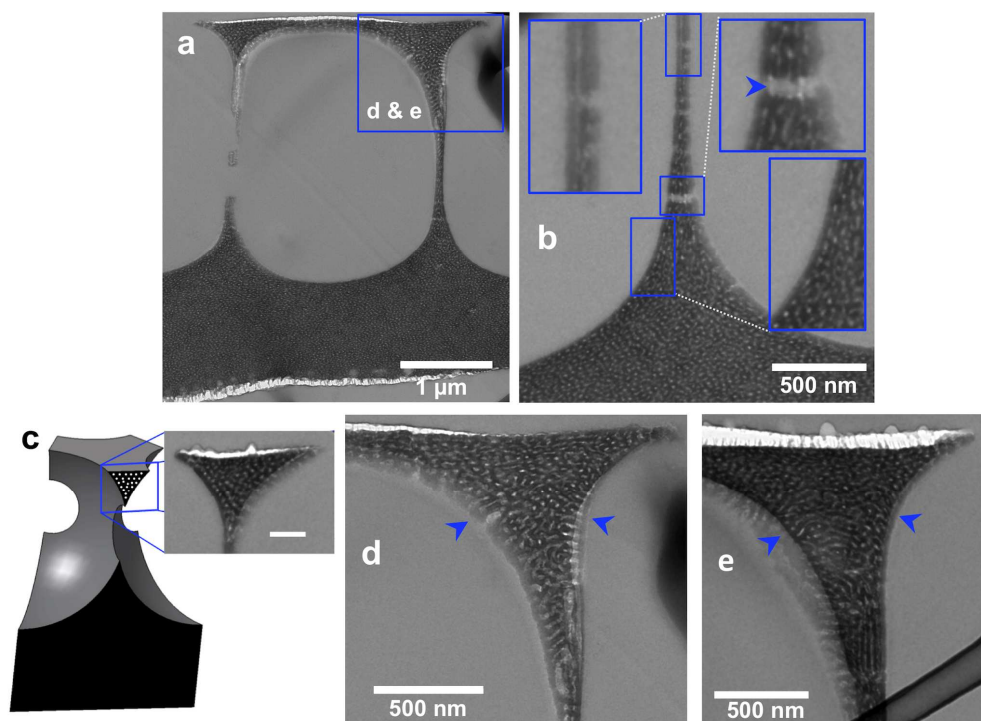


Fig. 5 Cryo-TEM images collected on P_{CVL} HC films stained with RuO_4 and schematic representation of a HC film section (c). The delimited region in (a) corresponds to blowup (d). TEM image (e) is collected in a similar region as (d).

Discussion

The experimental data presented in the previous section demonstrate the relations between the nano- and micrometer length scale self-organization. To better describe and analyze this interplay the film formation process is decomposed in with five identified physical mechanisms: (i) the water droplet nucleation, growth and packing on top of the evaporating polymer solution;²³ (ii) the polymer solution flows provoked by the water spheres sinking¹⁰ and droplet arrays motion;⁹ (iii) the copolymer self-assembly driving force related to the product χN , with χ the Flory-Huggins parameter and N the polymer degree of polymerization;^{24, 25} (iv) the solvent evaporation and the slight solvent blocks selectivity;^{26, 27} and finally (v) the affinity of both pure polymers with water related to their surface free energies.

Sample P_{LAM} presents a high degree of lamellar ordering around the pores (onion-like morphology) driven by a preferential affinity between the PS blocks and the former water droplets interface as observed on the TEM images (Fig. 4 c). Indeed, considering the surface free energy of pure PS and pure PtBA (about 40 and 30 $\text{mN}\cdot\text{m}^{-1}$ respectively at 20 °C)^{28, 8} a lower water contact angle is expected for solid PS using the Girifalco and Good expression²⁹ in the Young equation.

The second recurrent feature noticed on the P_{LAM} film is the double layers configuration (Fig. 4 b & d), *i.e.* long range ordering around the pores (upper region 1) and short range ordering (lower region 2). This structure is analyzed as a

signature of a past mechanical stresses,³⁰ and more precisely here, the droplet array tectonic occurring during the film formation, recently proposed by M. Shimomura and coworkers.⁹

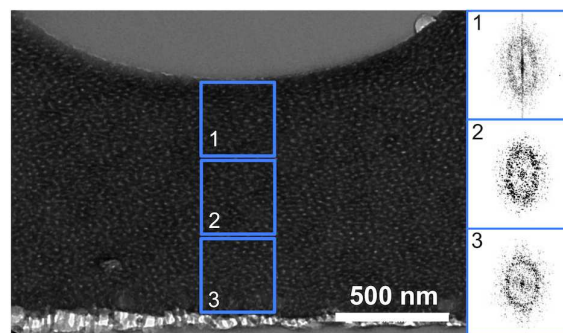
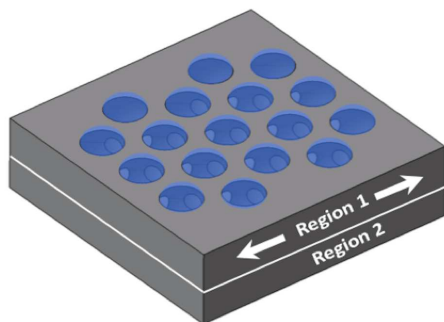


Fig. 6 Cryo-TEM images collected on RuO_4 -stained P_{CVL} HC film (extracted from Fig. 5 b). The three insets on the right present the 2D FFTs calculated from the delimited regions ($400 \times 400 \text{ nm}^2$) with corresponding numbers.

The two regions are respectively associated to a former upper solid layer, presenting a depleted solvent content, and a lower viscous layer, with a higher solvent content. Such solvent concentration gradient is in agreement with the profile expected in evaporating polymer solutions.^{31, 32} The upper solid layer containing the water droplets and already nano-structured, can drift on top of the viscous layer, which undergoes an important mechanical stress limiting the long-range copolymer ordering (Schema 1).

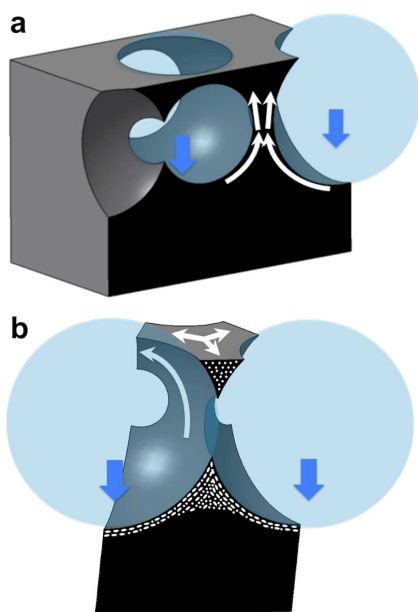
Copolymer P_{CYL} has a limited capability to self-segregate with a long range ordering during the rapid Breath Figure process compared to P_{LAM} . The hexagonal packed cylinders structure revealed by SAXS on the thermally annealed continuous film is no longer observed on the HC film. This dissimilarity between P_{LAM} and P_{CYL} can be explained by their difference of S/tBA composition and their total molar masses, leading to a significantly higher estimated χN value for P_{LAM} than P_{CYL} (Table 1). This χN discrepancy is assumed to be maintained during the film formation considering the dilution approximation.³³ However, the P_{CYL} morphology can be depicted as dispersed worm-like nano-domains presenting collective and recurrent orientations. In parallel, at the micrometer length scale, P_{CYL} polymer leads systematically to HC films of higher quality (*i.e.* lower entropy value) compare to P_{LAM} . The probable reason is a difference in solution viscosity during the evaporation process, which directly impacts the droplet mobility. Indeed, the expected increase of viscosity, with the substantial copolymer self-aggregation³⁴ associated to the high degree of ordering of P_{LAM} , is a limiting factor to reach the micrometer droplet's optimum hexagonal packing.



Scheme 1. Schematic representation of the droplet array tectonic occurring during the film formation. The upper solid region 1 containing the water droplets can drift on top of the viscous region 2.

Specific orientations of the worm-like domains are noticed around the pores on sample P_{CYL} (Fig. 6). This variation of orientation, *i.e.* parallel or orthogonal to the interfaces, demonstrates that the preferential affinity of PS domains toward the former water droplets is not the predominant driving force during the self-assembly process. Moreover, identical fluctuations of orientation are observed around all the pores, which supposes kinetically trapped structures resulting of similar self-assembly mechanisms occurring around each water droplet. To analyze the worm-like domain orientations as traces of the past Breath Figure process, the anisotropic PtBA domains have to be partially formed within a range of polymer concentration prior the final glassy state. Indeed, considering that the solvent is of slightly higher quality for the PS majority phase than for PtBA,^{35,36} the polymer solution is expected to undergo disorder-to-order transition during the evaporation process.^{26, 27} The kinetically trapped orientations observed on the TEM pictures are then exploited as imprints of the ultimate flows occurring during the Breath Figure process and resulting from the collective droplets sinking into the polymer solution.^{10, 11} Around the lower hemisphere of the sinking droplets, the polymer solution is under pressure and flows upward (Scheme 2 a), which is in agreement with the domains oriented along compacted plans fitting the interface over few periods and vanishing deeper in the bulk (Fig. 6). On the other hand, around the upper hemisphere of the sinking droplets, the pressure is lower and the flow lines leave the interface (scheme 2 a), which is in agreement with the nano-domains oriented orthogonally to the interface, as pointed by blue arrows on Fig. 5 d & e. It is worth to note that this orthogonal orientation is observed only when an upward solution flow is possible, *i.e.* when a thick polymer wall is present underneath. Indeed, the isolated upper regions (Fig. 5 c) present a domain orientation orthogonal to the TEM section plan. This is also in agreement with the expected horizontal solution flow when the droplets are sinking (white arrows on Scheme 2 b).

The analysis conducted on both polymer HC films demonstrates that the nanostructure orientation and ordering are consistent with the expected solution flow occurring when the droplets are sinking and with tectonic effect. The efforts are pursued to consolidate this multi-scale approach and also to extract further information from the nano-structure such as: the formation of HC multilayer, the merging process of droplets controlling the connectivity between the pores, and to demonstrate the occurring of the Benard-Marangoni convections flows driven by the temperature gradient.



Scheme 2. Schematic representations of the polymer solution flows (white arrows) when the water droplets are sinking (blue arrows). Scheme (a) corresponds to the configuration of TEM section Fig. 5 a and scheme (b) corresponds to the configuration of Fig. 5 c.

Conclusions

The present work shows that highly order and oriented coil-coil copolymer nano-structures can be achieved in the entire honeycomb films obtained by the fast solvent evaporation Breath Figure process, *i.e.* out of thermodynamical equilibrium. Interestingly, the exposed data reveal an interaction between the nano- and the micrometer length scale self-organization processes, especially through the formation of the water droplets / evaporating polymer solution interface and the droplet collective motions. Those interactions establish the potential interest of using the kinetically trapped block copolymer self-organization as an imprint to elucidate the complex HC film formation. Indeed, the nano-structures ordering and orientation are inhomogeneous in the TEM sections with significant differences between both studied polymers. The copolymer leading to lamellae reveals a strong influence of the interfaces with a regular orientation of the lamellae around the pores (onion-like morphology) together with heterogeneity in the continuous film underneath the porosity analyzed as a trace of the water droplets lateral displacement, *i.e.* tectonic effect. On the other hand, the copolymer leading to worm-like domains presents a variety of orientations around the pore exploited as imprints of the ultimate flows occurring during the collective droplets sinking. At this point, fluid dynamics simulation would be a pertinent and complementary approach to confirm the polymer solution flows occurring with the water droplets collective motion. To conclude, the knowledge and control of the nano-structure orientation in the different regions of the HC film become crucial when considering interfacial properties

such as triggered wettability, adhesion, cell growth or photonics, just to mention some potential applications.

Acknowledgements

The authors are grateful for the financial support of Conseil Général 64 and Région Aquitaine is acknowledged for P.E. PhD funding. L.B., P.E. and L.R. thank the European Science Foundation (ESF) through Precision Polymer Materials (P2M) network for visiting grants at Aalto University. L.R. thanks the CNRS for his Délégation fellowship. We are thankful to Léon Brillouin Laboratory (LLB) and European Synchrotron Research Facility (ESRF) for neutron and X-ray, as well as the local contacts A. Lapp (PAXY) and M. Fernandez (ID02) for their help. L. Marlin (UPPA) is thanked for his 3D figure inputs.

Notes and references

‡ The TEM image collected on sample RuO₄ stained P_{CYL} (Fig. 5 c) demonstrates a marked contrast between the clear PtBA filaments in the stretched wall (pointed by arrow in the upper right inset) and the darker grey resin. It is then possible to ascribe a grey scale for the three components: black for the PS, dark grey for the resin and light grey for the PtBA.

§ Values estimated from PS 44000 (40.7 mN.m⁻¹) and PnBA (30.7 mN.m⁻¹) & PtBMA (30.4 mN.m⁻¹) both relatively close to PtBA.

§§ The relative solvent qualities are estimated from the solubility parameters (18.2 and 16.4 MPa^{1/2} for PS and PtBA respectively) versus CS₂ (20.5 MPa^{1/2}).³²

1. B. Francois, O. Pitois and J. Francois, *Adv. Mater.*, 1995, **7**, 1041-1044.
2. G. Widawski, M. Rawiso and B. Francois, *Nature*, 1994, **369**, 387-389.
3. U. H. F. Bunz, *Adv. Mater.*, 2006, **18**, 973-989.
4. M. H. Stenzel, C. Barner-Kowollik and T. P. Davis, *J. Polym. Sci. Pol. Chem.*, 2006, **44**, 2363-2375.
5. M. Hernandez-Guerrero and M. H. Stenzel, *Polymer Chemistry*, 2012, **3**, 563-577.
6. P. Escalé, L. Rubatat, L. Billon and M. Save, *European Polymer Journal*, 2012, **44**, 9.
7. A. Muñoz-Bonilla, M. Fernández-García and J. Rodríguez-Hernández, *Prog. Polym. Sci.*, 2014, **39**, 510-554.
8. H. Iwanaga, K. Shiratsuchi and H. Yamazaki, *Fujifilm Research & Development*, 2009, **54**, 43-47.
9. H. Yamazaki, K. Ito, H. Yabu and M. Shimomura, *Soft Matter*, 2014, **10**, 2741.
10. M. Srinivasarao, *Science*, 2001, **292**, 79-83.
11. L. Song, V. Sharma, J. O. Park and M. Srinivasarao, *Soft Matter*, 2011, **7**, 1890.
12. L. F. Boesel, C. Greiner, E. Arzt and A. del Campo, *Adv. Mater.*, 2010, **22**, 2125-2137.
13. T. Verho, C. Bower, P. Andrew, S. Franssila, O. Ikkala and R. H. A. Ras, *Adv. Mater.*, 2010.

14. B. Bhushan and Y. C. Jung, *Prog. Mater. Sci.*, 2011, **56**, 1-108.
15. P. Escalé, M. Save, A. Lapp, L. Rubatat and L. Billon, *Soft Matter*, 2010, **6**, 3202-3210.
16. T. Hayakawa and S. Horiuchi, *Angewandte Chemie-International Edition*, 2003, **42**, 2285-2289.
17. A. Munoz-Bonilla, E. Ibarboure, E. Papon and J. Rodriguez-Hernandez, *Langmuir*, 2009, **25**, 6493-6499.
18. P. Escalé, L. Rubatat, C. Derail, M. Save and L. Billon, *Macromolecular Rapid Communications*, 2011, **32**, 1072-1076.
19. P. Escalé, W. Van Camp, F. Du Prez, L. Rubatat, L. Billon and M. Save, *Polymer Chemistry*, 2013, **4**, 4710-4717.
20. S. Chen, M.-H. Alves, M. Save and L. Billon, *Polymer Chemistry*, 2014, **5**, 5310-5319.
21. L. Ghannam, M. Manguian, J. Francois and L. Billon, *Soft Matter*, 2007, **3**, 1492-1499.
22. P. Debye, J. H.R. Anderson and H. Brumberger, *J. Appl. Phys.*, 1957, **28**, 679.
23. O. Pitois and B. Francois, *Colloid Polym. Sci.*, 1999, **277**, 574-578.
24. L. Leibler, *Macromolecules*, 1980, **13**, 1602-1617.
25. M. W. Matsen and F. S. Bates, *Macromolecules*, 1996, **29**, 1091.
26. T. P. Lodge, M. W. Hamersky, K. J. Hanley and C.-I. Huang, *Macromolecules*, 1997, **30**, 6139-6149.
27. T. P. Lodge, K. J. Hanley, B. Pudil and V. Alahapperuma, *Macromolecules*, 2003, **36**, 816-822.
28. *Polymer Handbook* Wiley, 4th edn., 2003.
29. L. A. Girifalco and R. J. Good, *Journal of Physical Chemistry*, 1957, **61**, 904-909.
30. J.-H. Lee, D. Veyssset, J. P. Singer, M. Retsch, G. Saini, T. Pezeril, K. A. Nelson and E. L. Thomas, *Nature Communications*, 2012, **3**, 1164.
31. M. Tsige and G. S. Grest, *Macromolecules*, 2004, **37**, 4333-4335.
32. S. H. Kim, M. J. Misner, T. Xu, M. Kimura and T. P. Russell, *Adv. Mater.*, 2004, **16**, 226-231.
33. E. Helfand and Y. Tagami, *The Journal of Chemical Physics*, 1972, **56**, 3592-3601.
34. J. C. Kim, M. Seo, M. A. Hillmyer and L. F. Francis, *ACS Applied Materials & Interfaces*, 2013, **5**, 11877-11883.
35. *Physical Properties of Polymer Handbook*, Springer, 2nd edn., 2007.